

Strong horizontal internetwork magnetic field: numerical simulations in comparison to observations with Hinode

O. Steiner and R. Rezaei

Kiepenheuer-Institut für Sonnenphysik, Schöneckstrasse 6, D-79104 Freiburg, Germany

[steiner,rrezaei]@kis.uni-freiburg.de

W. Schaffenberger

Physics and Astronomy Department, Michigan State University, East Lansing, MI 48824

schaffen@pa.msu.edu

and

S. Wedemeyer-Böhm¹

Institute of Theoretical Astrophysics, P.O. Box 1029, Blindern, N-0316 Oslo, Norway

sven.wedemeyer@astro.uio.no

ABSTRACT

Solar observations with the Hinode space observatory led to the discovery of strong horizontal magnetic fields in the photosphere of quiet internetwork regions. Here we investigate realistic numerical simulations of the surface layers of the Sun with respect to horizontal magnetic fields and compute the corresponding responses in the Fe I 630 nm line pair. We analyze two simulation runs with greatly different initial and boundary conditions. Both show a local maximum in the mean flux density of the horizontal field component at a height of around 500 km in the photosphere, where the horizontal surpasses the vertical component by a factor of 2.0 or 5.6, depending on the initial and boundary conditions. From the synthesized Stokes profiles we derive a mean horizontal field component that is, respectively, 1.5 and 2.8 stronger than the vertical component. This is the consequence of both intrinsically stronger flux densities and the larger area fraction occupied by, the horizontal fields. It is shown that convective overshooting pumps horizontal fields in the vertical direction, leading to a positive vertical

¹Marie Curie Research Fellow

Poynting flux in the photosphere, while this quantity is negative in the convectively unstable layer below it so that the solar surface constitutes a separatrix for the vertical Poynting flux.

Subject headings: Sun: photosphere — Sun: magnetic fields — MHD — polarization — turbulence

1. Introduction

Recent observations with the spectropolarimeter of the Solar Optical Telescope (SOT) onboard the Hinode space observatory show that quiet internetwork regions (the inner regions of supergranular cells of the quiet Sun) harbor photospheric magnetic field whose mean flux density of the horizontal component considerably surpasses that of the vertical component (Lites et al. 2008, 2007). According to this paper, the vertical fields are concentrated in the intergranular lanes, whereas the stronger, horizontal fields occur most commonly at the edges of the bright granules, aside from the vertical fields.

In a gravitationally stratified atmosphere, vertical magnetic flux concentrations naturally develop a horizontal component as they expand with height in a funnel-like manner. Indeed, also from Hinode data, Rezaei et al. (2007) found a conspicuous pattern in the area asymmetry of Stokes- V profiles, which they trace back to funnel shaped magnetic flux concentrations in the internetwork. However, the horizontal fields discovered by Lites et al. (2008, 2007) also occur apart from vertical flux concentrations and they seem to cover a larger area fraction than the vertical fields.

In order to gain understanding of the nature of these horizontal fields, we have carried out an analysis of existing and new data from three-dimensional magnetohydrodynamic computer simulations of internetwork magnetic fields. The aim was to answer the following questions: Does a realistic simulation of the surface layers of the Sun intrinsically produce horizontal magnetic fields and can their mean flux density indeed surpass the mean flux density of the vertical field component? Can this field be reliably measured with Zeeman effect based polarimetry?

In the following we explain in Sect. 2 the details of two runs that differ in their initial state and boundary conditions and present results that answer the first two of the above questions in Sect. 3. In Sect. 4, we synthesize Stokes profiles from the simulation data and compare them to the measurements of Lites et al. (2008, 2007) from Hinode. Conclusions and discussion follow in Sect. 5.

2. Two simulation runs

We have carried out two runs, run v10 and run h20, which significantly differ in their initial and boundary conditions for the magnetic field. This enables us to judge the robustness of our results with respect to magnetic boundary conditions. Both runs are carried out within a common three-dimensional computational domain encompassing the integral layers from the upper convection zone to the middle chromosphere. The height range extends over 2800 km, from 1400 km below the mean surface of optical depth unity to 1400 km above it. With this choice we assure that the top boundary lies far away from the low photosphere, where the spectral lines that were used for the measurements with Hinode form. The horizontal dimensions are $4800 \times 4800 \text{ km}^2$, corresponding to $6.6'' \times 6.6''$ on the solar disk. With 120^3 grid cells, the spatial resolution in the horizontal direction is 40 km, while in the vertical direction it is 20 km throughout the photosphere and chromosphere, increasing to 50 km through the convection-zone layer. In both runs the lateral boundary conditions are chosen to be periodic in all variables, whereas the bottom boundary is “open” in the sense that the fluid can freely flow in and out of the computational domain under the condition of vanishing total mass flux. Thereby, the specific entropy of the inflowing mass is fixed to a value previously determined so as to yield solar radiative flux at the upper boundary. The upper boundary is “closed” in run v10, i.e., reflecting boundaries are applied to the vertical velocity. Run h20 features “open” top conditions.

The two runs differ most significantly in the initial state and boundary conditions for the magnetic field. Run v10 starts with a homogeneous, vertical, unipolar magnetic field of a flux density of 1 mT superposed on a previously computed, relaxed model of thermal convection. After relaxation, fields of mixed polarity occur throughout the photosphere with an area imbalance of typically 3:1 for fields stronger than 1 mT. Similar polarity imbalances of even larger fields of view also occur in observational data of the internetwork (Lites 2002).

The magnetic field in run v10 is constrained to have vanishing horizontal components at the top and bottom boundary but lines of force can freely move in the horizontal direction to the boundaries. Although this condition is quite stringent for the magnetic field near the top boundary, it still allows the field to freely expand with height through the photospheric layers, different from conventional simulations that extend to a height of typically 600 km only. The mean vertical net magnetic flux density remains 1 mT throughout the simulation. These magnetic boundary conditions might actually be more appropriate for the simulation of network magnetic fields because of the preference for one polarity and the vertical direction.

Run h20 starts without a magnetic field but fluid that enters the simulation domain across the bottom boundary area carries horizontal magnetic field of a uniform flux density of 2 mT and of uniform direction parallel to the x -axis. Outflowing material carries whatever

magnetic field it happens to have. These boundary conditions are the same as used by Stein & Nordlund (2006). They are appropriate when flux emerges from deeper layers of the convection zone. Starting from a relaxed model of thermal convection, magnetic field steadily spreads into the convective layer of the simulation domain, where it gets strengthened by the convective plasma motion and reaches the surface of optical depth unity, $\tau_{500\text{nm}} = 1$, after 600 s. From then on magnetic field slowly begins to expand throughout the photosphere, growing in mean absolute strength. The field can cross the top boundary at any angle under the condition $dB_{x,y,z}/dz = 0$.

Figure 1 shows the growth of magnetic energy in the computational box of run h20 over the total simulation time of 3.34 h. It also shows the mean absolute vertical magnetic field strength at a fixed geometrical height corresponding to the mean optical depth unity. Starting from zero, the magnetic energy steadily increases because energy is transferred from convective kinetic to magnetic and because of the upwellings, which continuously advect magnetic field into the box. But increasingly, events of plumes pump magnetic fields in the downward direction out of the domain and after a time of about 2.45 h a maximum value is reached and an equilibrium in the transport of magnetic energy across the bottom boundary establishes itself. At this time, the absolute magnetic flux density near the surface of optical depth $\tau_{500\text{nm}} = 1$ is approximately 1 mT.

Runs v10 and h20 have been carried out with an extended version of the computer code CO⁵BOLD that includes magnetic fields. The code solves the coupled system of the equations of compressible ideal magnetohydrodynamics in an external gravity field with non-local, frequency-independent radiative transfer. The multidimensional problem is reduced to a sequence of 1-D sweeps by dimensional splitting. Each of these 1-D problems is solved with a Godunov-type finite-volume scheme using an approximate Riemann solver modified for a realistic equation of state and gravity. Details of the method can be found in Schaffenberger et al. (2005, 2006).

3. Structure and development of the horizontal magnetic field

Figure 2 shows the horizontally and temporally averaged absolute vertical and horizontal magnetic flux density as functions of height for both runs. In run h20, the mean horizontal field strength, $\langle \sqrt{B_x^2 + B_y^2} \rangle$, is larger than the mean strength of the vertical component, $\langle B_z \rangle$, throughout the photosphere and the lower chromosphere, in run v10 between 250 km and 850 km height. It shows a local maximum close to the classical temperature minimum at a height of around 500 km, where it is 5.6 times stronger than the mean vertical field in case of run h20. The horizontal fields also dominate in the upper photosphere of run v10 for which

case one might expect the initial state and boundary condition to favor the development of vertical fields rather than horizontal ones. There, the ratio $\langle B_{\text{hor}} \rangle / \langle B_{\text{ver}} \rangle$ at the location of maximum $\langle B_{\text{hor}} \rangle$ is 2.5.

Figure 3 shows for a typical time instant in the second half of run h20 the horizontal field strength (colors) in a horizontal section at a height of mean optical depth unity. Superimposed on the color scale are contours of 3 mT of the vertical field strength, where solid and dashed contours have opposite polarity. The area covered by horizontal fields stronger than 5 mT is 17.2 % of the total area, while this fraction is 4.3 % for the vertical fields surpassing 5 mT. The corresponding temporal averages for the second half of the h20 time series, are 14.2 % and 5.1 %, respectively. At the height of 200 km in the photosphere and a threshold of 2 mT the average area fractions are 25.8 % for the horizontal field component and 6.2 % for the vertical one. Thus, fields with a horizontal component larger than a given limit in strength occupy a significantly larger area fraction than fields with a vertical component exceeding this limit. This is a second reason (after inherent strength) why the measured mean flux density of the horizontal field component may exceed that of the vertical component.

Still in Fig. 3, to the right and the lower right direction from the center as well as in the middle close to the lower boundary, we can see a frequently occurring event consisting of a “ring” of horizontal field. It starts to appear as a patch filled with horizontal field within a granule, subsequently expanding to become a ring. The ring can also be seen in the vertical field component, where opposite halves of it have opposite polarity as is visible from the indicated 3 mT contours. This pattern arises from horizontal magnetic field that is transported to the surface by warm upflows. The field is anchored in the downdrafts at the edges of the growing granule or in the weaker upwellings of a granule interior. The horizontal field is strongest near these edges, where the field is most concentrated. Typically a ring does not enclose a full granule but only part of it so that part of the vertical magnetic field occurs within the granule. The horizontal field between the crescents of vertical fields of opposite polarity covers part of the granule like a cap forming a small-scale canopy, as was shown before in Schaffenberger et al. (2005) and Schaffenberger et al. (2006). Observationally, similar events were detected by Centeno et al. (2007).

In the higher layers of the atmosphere, the horizontal field covers the entire ring interior, as we know from horizontal sections like that of Fig. 3 but of ever increasing height. Part of this horizontal field is pushed further into the stable layers of the photosphere by the overshooting convection. There, it stops rising for lack of buoyancy, neither is it pumped back in the downward direction for lack of strong downflow plumes. As a consequence, this process leads to an accumulation of horizontal fields in the upper photosphere and lower chromosphere. Granular flow and the overshooting convection act to expel magnetic flux

from the granule interior to its boundaries, i.e., the intergranular lanes but also the upper layers of the photosphere.

Indeed, the surface of optical depth unity, which separates the convective regime from the subadiabatically stratified photosphere, also acts as a separatrix for the vertically directed Poynting flux, S_z , where

$$S = \frac{1}{4\pi}(\mathbf{B} \times (\mathbf{v} \times \mathbf{B})). \quad (1)$$

This can be seen in Fig. 4 (top), which displays the horizontally averaged S_z as a function of height in the atmosphere and time for the second half of run h20. The conspicuous dark streaks in the lower part of the diagram mark events of downflow plumes that carry horizontal magnetic field with them, giving rise to $\langle S_z \rangle < 0$. Above the surface of $\tau_{500\text{ nm}} = 1$, $\langle S_z \rangle$ stays mainly positive (bright), due to the transport of horizontal fields in the upward direction. This can also be seen from the middle panel of Fig. 4, which shows the horizontal magnetic field strength as a function of time and height. Again, most conspicuous are horizontal fields that are pumped in the downward direction within the convection zone, but also visible are events of horizontal fields being transported upwards from the surface by convective overshoots. They become deposited in and give rise to the distinct layer of enhanced horizontal fields in the upper photosphere. This layer is separated from the convection zone by the layer of overshooting convection. The bottom panel of Fig. 4 shows the mean vertical field strength that monotonically decreases with height at all times.

4. Comparison with results from the Hinode space observatory

In the previous section we have seen that the simulations produce a strong horizontal magnetic field in the photosphere. Its functional dependency on height differs from that for the vertical field component and also the area fill fractions for the two components differ. Hence, the response of this field in linear and circular Zeeman polarization is not a trivial one.

For a comparison with Zeeman measurements with the Hinode spectropolarimeter we therefore synthesized the Stokes profiles of both 630 nm Fe I spectral lines for the two simulation runs. Profiles were computed with the radiative transfer code SIR (Ruiz Cobo & del Toro Iniesta 1992; Bellot Rubio 2003) along vertical lines of sight (corresponding to an observation at disk center) with a spectral sampling of 2 pm. For a faithful comparison with the results of Lites et al. (2008), we subject the synthetic profiles to the same procedure for conversion to “apparent flux density” as was done by Lites et al.. Thus, we obtain calibration curves for the conversion from the wavelength integrated polarization signals V_{tot}

and Q_{tot} to the apparent longitudinal and transversal magnetic flux densities $|B_{\text{app}}^{\text{L}}|$ and $B_{\text{app}}^{\text{T}}$, respectively. Equally, Q_{tot} is the resulting Q -profile after transformation to the “preferred-frame azimuth” in which the $+Q$ -direction is parallel to the projection of the magnetic field vector on the plane of sky, when $U \approx 0$.

The only difference to Lites et al. (2008) is that we use a different radiative transfer code (SIR vs the ASP code) and that we use the temporally and spatially averaged atmosphere of run v10 for the derivation of the calibration curves, for which Lites et al. used a Milne-Eddington atmosphere. For control purposes we also computed calibration curves with the HSRA standard atmosphere and the temporally and spatially averaged atmosphere of run h20 but found no difference below 120 mT. Also, our Q_{mask} (a weighting function for the computation of Q_{tot}) is the normalized average over all the synthetic Q -profiles in the “preferred-frame”, exactly as was done by Lites et al. (2008) with respect to the observed profiles.

Having the calibration curves, we derive spatial and temporal averages for the transversal and longitudinal apparent magnetic flux densities, $B_{\text{app}}^{\text{T}}$ and $|B_{\text{app}}^{\text{L}}|$ of respectively 24.8 Mx cm^{-2} and 8.8 Mx cm^{-2} for the second half of run h20 and 11.5 Mx cm^{-2} and 7.5 Mx cm^{-2} for run v10. Thus, the ratio $\langle B_{\text{app}}^{\text{T}} \rangle / \langle |B_{\text{app}}^{\text{L}}| \rangle = 2.8$ in case of run h20 and 1.5 in case of run v10. Lites et al. (2008) obtain from Hinode SP data $\langle |B_{\text{app}}^{\text{T}}| \rangle = 55 \text{ Mx cm}^{-2}$ and $\langle |B_{\text{app}}^{\text{L}}| \rangle = 11 \text{ Mx cm}^{-2}$ resulting in $\langle B_{\text{app}}^{\text{T}} \rangle / \langle |B_{\text{app}}^{\text{L}}| \rangle = 5.0$.

While $\langle B_{\text{hor}} \rangle / \langle B_{\text{ver}} \rangle = 5.6$ and 2.5 for run h20 and v10, respectively, at the location of maximum $\langle B_{\text{hor}} \rangle$, the above quoted lower ratios result because the main contribution to the Stokes signals does not come from this height but rather from the low photosphere. Only a minor contribution comes from the strong horizontal fields in the upper photosphere and lower chromosphere. Consequently, these results suggest that the true ratio of mean horizontal to vertical field strength in the upper photosphere may be even higher than the factor 5 derived by Lites et al. (2008) for the apparent flux densities. All this indicates that the photospheric magnetic field in the internetwork is highly anisotropic, different from the assumption of a homogeneously turbulent magnetic field, which interpretations of Hanle depolarization measurements usually rely upon.

5. Conclusion and discussion

We have carried out two realistic simulations of magnetoconvection in the surface layers of the quiet internetwork region of the solar atmosphere. The simulations greatly differ in their initial state and boundary conditions for the magnetic field, but otherwise they

both start from the same physical principles and both faithfully reproduce properties of normal granulation (as the magnetic field is weak). Both simulations intrinsically produce a horizontal magnetic field throughout the photosphere and lower chromosphere with a mean field strength that is comparable to or exceeding the mean flux density of the local vertical field component by up to a factor of 5.6. In a horizontal section at a height of mean optical depth unity, fields with a horizontal component exceeding 5 mT cover about three times more area than fields with a vertical component exceeding this limit.

Strong horizontal photospheric magnetic field in simulations were previously reported by Grossmann-Doerth et al. (1998) in a two-dimensional environment, who note: “... we find in all simulations also strong horizontal fields above convective upflows ...”, and by Schaffenberger et al. (2005, 2006) who describe the phenomenon of “small-scale canopies” in their three-dimensional simulations. They point to possibly significant ohmic dissipation of sheets of horizontal fields in the lower chromosphere. More recently, Schüssler & Vögler (2008) find predominant horizontal magnetic fields in the photosphere of a three-dimensional surface-dynamo simulation. Their closed top boundary lies at a height of only 500 km, which, judging from the present simulations, might strongly influence (force) the formation of horizontal fields in the photospheric layers immediately beneath it since this top boundary prevents them from extending above this limit. This estimate is corroborated by the 3-D simulations of Abbott (2007), which display “horizontally directed ribbons of magnetic flux that permeate the model chromosphere”, not unlike to the figures shown by Schaffenberger et al. (2006).

The horizontal field in the present simulation can be considered as a consequence of the flux expulsion process (Galloway & Weiss 1981): in the same way as magnetic flux is expelled from the granular interior to the intergranular lanes, it also gets pushed to the middle and upper photosphere by overshooting convection, where it tends to form a layer of horizontal field of enhanced flux density reaching up into the lower chromosphere. Below the surface of optical depth unity ($\tau_{500\text{ nm}} > 1$), convective plumes pump horizontal magnetic field in the downward direction. Hence, the surface of $\tau_{500\text{ nm}} = 1$, which separates the convective regime from the subadiabatically stratified photosphere, also acts as a separatrix for the vertically directed Poynting flux, which is mainly directed upwards above this surface and in the downward direction below it.

The response of the horizontal field in the linear and circular polarization of the two iron lines at 630 nm is with $\langle B_{\text{app}}^{\text{T}} \rangle / \langle |B_{\text{app}}^{\text{L}}| \rangle = 1.5$ to 2.8, less pronounced in the simulations than in the measurements by Lites et al. (2008), which indicate a factor of 5. One reason might be that (as a consequence of the arbitrarily chosen initial condition) the mean flux density in the simulations are smaller than what was measured by Lites et al. (2008), another the

finite spatial resolution of the simulation that prevents intermittence on a scale smaller than the horizontal grid resolution of 40 km. On the observational side, finite spatial resolution could possibly underestimate the mean absolute vertical field component because of polarity cancellation.

The strength of the horizontal field component shows a local maximum close to the classical temperature minimum near 500 km height, which largely escapes measurements with the iron line pair at 630 nm. This indicates that the horizontal component of the internetwork magnetic field in the upper photosphere may be even stronger than the flux densities measured with the help of the Fe I 630 nm spectral lines. It can also be reassured that the mean apparent flux densities derived from the total polarization of the synthesized Stokes profiles is in good agreement with the true mean flux densities found in the simulation in the formation range of these lines.

The authors thank R. Hammer for detailed comments on a draft version of this paper. This work was supported by the Deutsche Forschungsgemeinschaft (SCHM 1168/8-1).

REFERENCES

Abbett, W. P. 2007, *ApJ*, 665, 1469

Bellot Rubio, L. R. 2003, Inversion of Stokes profiles with SIR, (Freiburg: Kiepenheuer Institut für Sonnenphysik)

Centeno, R., Socas-Navarro, H., Lites, B., Kubo, M., Frank, Z., Shine, R., Tarbell, T., Title, A., Ichimoto, K., Tsuneta, S., Katsukawa, Y., Suematsu, Y., Shimizu, T., & Nagata, S. 2007, *ApJ*, 666, L137

Galloway, D. J., & Weiss, N. O. 1981, *ApJ*, 243, 945

Grossmann-Doerth, U., Schüssler, M., & Steiner, O. 1998, *A&A*, 337, 928

Lites, B. W. 2002, *ApJ*, 573, 431

Lites, B. W., Kubo, M., Socas-Navarro, H., Berger, T., Frank, Z., Shine, R., Tarbell, T., Title, A., Ichimoto, K., Katsukawa, Y., Tsuneta, S., Suematsu, Y., Shimizu, T., & Nagata, S. 2008, *ApJ*, 672, 1237

Lites, B. W., Socas-Navarro, H., Kubo, M., Berger, T., Frank, Z., Shine, R., Tarbell, T., Title, A., Ichimoto, K., Katsukawa, Y., Tsuneta, S., Suematsu, Y., Shimizu, T., & Ngata, S. 2007, *PASJ*, 59, 571

Rezaei, R., Steiner, O., Wedemeyer-Böhm, S., Schlichenmaier, R., Schmidt, W., & Lites, B. W. 2007, *A&A*, 476, L33

Ruiz Cobo, B., & del Toro Iniesta, J. C. 1992, *ApJ*, 398, 375

Schaffenberger, W., Wedemeyer-Böhm, S., Steiner, O., & Freytag, B. 2005, in *ESA Special Publication*, Vol. 596, Chromospheric and Coronal Magnetic Fields, ed. D. E. Innes, A. Lagg, & S. A. Solanki

Schaffenberger, W., Wedemeyer-Böhm, S., Steiner, O., & Freytag, B. 2006, in *ASP Conference Series*, Vol. 354, Solar MHD Theory and Observations, ed. J. Leibacher, R. F. Stein, & H. Uitenbroek, 345

Schüssler, M., & Vögler, A. 2008, ArXiv e-prints, 0801.1250

Stein, R. F., & Nordlund, Å. 2006, *ApJ*, 642, 1246

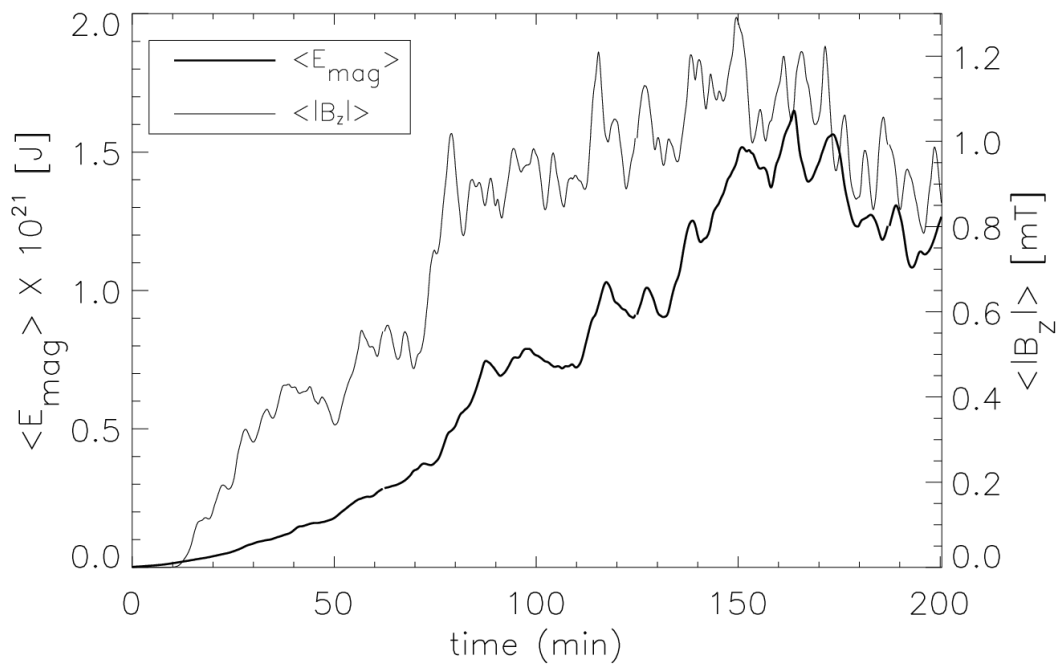


Fig. 1.— Total magnetic energy, E_{mag} , and horizontally averaged, absolute magnetic field strength, $\langle |B_z| \rangle$ ($\langle \tau_{500 \text{ nm}} \rangle = 1$), as functions of time for run h20.

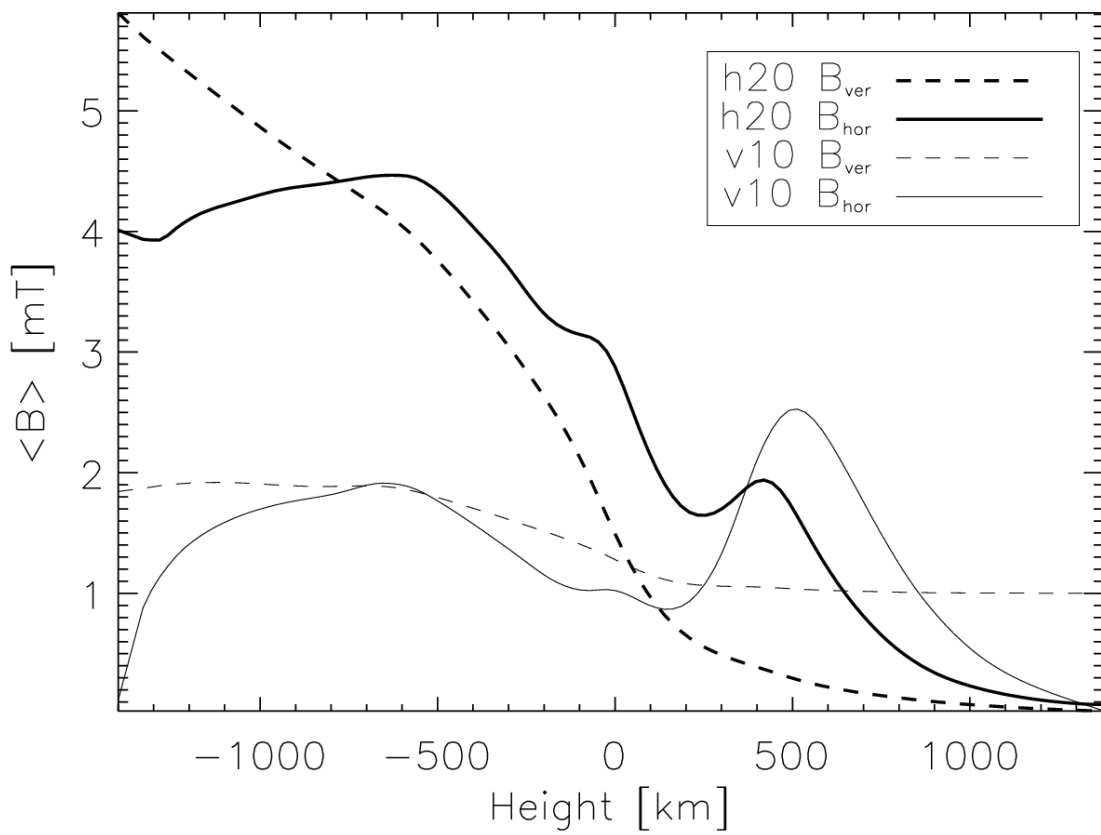


Fig. 2.— Horizontal (solid) and vertical (dashed) absolute field strength as functions of height for run h20 (heavy curves) and for run v10 (light curves).

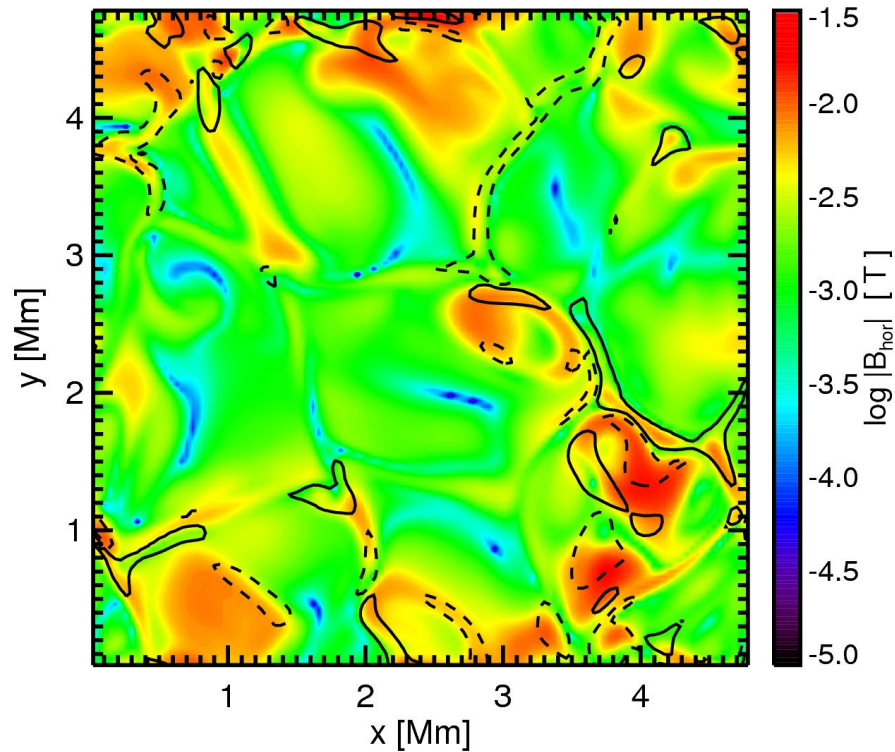


Fig. 3.— Horizontal field strength in a horizontal section at the height of mean optical depth unity at 500 nm. The black curves refer to contours of 3 mT vertical field strength, where solid and dashed contours have opposite polarity.

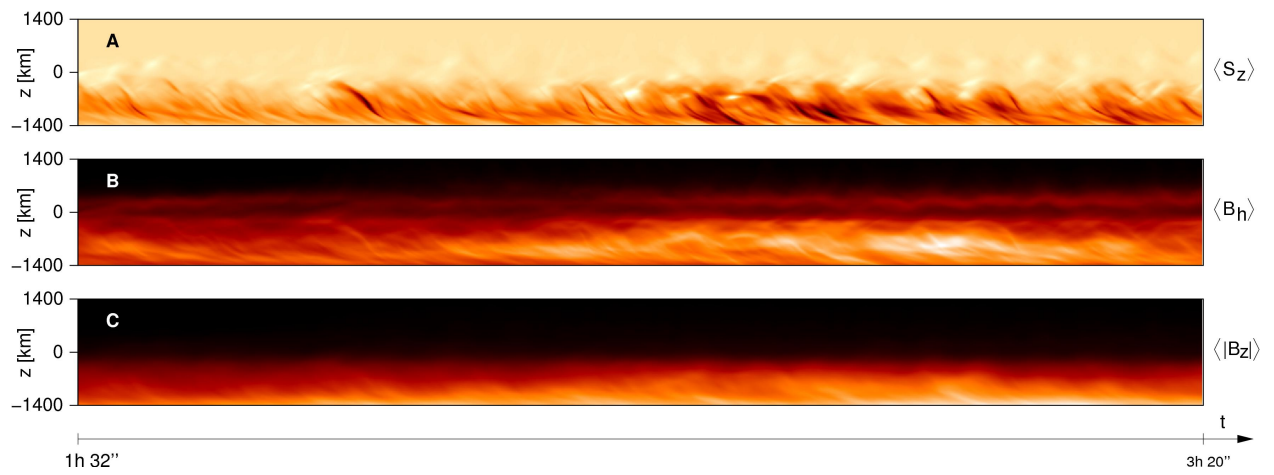


Fig. 4.— Vertically directed Poynting flux, S_z , horizontal magnetic flux density, $\langle B_h \rangle$, and vertical absolute magnetic flux density, $\langle |B_z| \rangle$ as functions of height and time from run h20. All quantities are averages in horizontal planes of the three-dimensional computational box.